Deriving ionospheric TEC by VGOS data analysis during CONT17

Sanam Motlaghzadeh[1], M. Mahdi Alizadeh[1,2], Roger Cappallo[3], Robert Heinkelmann[4], Harald Schuh[2,4]

[1] Faculty of Geodesy and Geomatics Eng., K. N. Toosi University of Technology, Tehran, Iran

[2] Institute of Geodesy and Geoinformation Sciences, Technical University of Berlin, Germany

[3] MIT Haystack Observatory, Westford, Massachusetts, United States

[4] German Research Centre for Geosciences (GFZ), Potsdam, Germany

Sanam Motlaghzadeh (motlaghzadeh@email.kntu.ac.ir), https://orcid.org/0000-0003-0895-2893

M. Mahdi Alizadeh (alizadeh@kntu.ac.ir)

Roger Cappallo (rjc@haystack.mit.edu)

Robert Heinkelmann (rob@gfz-potsdam.de)

Harald Schuh (schuh@gfz-potsdam.de)

Key points:

- We studied the variation of ionospheric Total Electron Content over six stations in December 2017 using VGOS data, new generation of VLBI.
- We used GIM data to evaluate our results, which enabled us to detect the sign error in the VGOS differential TEC data.
- By enhancing the model, we estimated the temporal variation of ionospheric gradient and achieve more accurate results.

Abstract

This article focuses on the new generation of *Very Long Baseline Interferometry* (VLBI), the *VLBI Global Observing System* (VGOS), and measurements carried out during CONT17 campaign. It uses broadband technology that increases both the number and precision of observations. These characteristics make VGOS a suitable tool for studying the atmosphere. This study focuses on the effects of the ionosphere on VGOS signals using a model that incorporates and extends ideas originally published in Hobiger et al. (2006). Our investigation revealed that the differential Total Electron Content (dTEC) data product calculated with the VGOS post-processing software revealed a sign error in the inferred dTEC values. Fortunately, this error does not change the final values of the phase and group delay. Therefore, this study was a way to identify this problem within the VGOS data. After diagnosing and solving this problem, the Hobiger et al. (2006) model was modified such that instead of considering a single unknown for the latitude gradient of the ionosphere, a time series of latitude gradients were taken into account. For comparison purposes, time series of Vertical Total Electron Content (VTEC) at each station during CONT17 campaign were constructed from Global Ionosphere Map (GIM) data. In this way, it is shown that the final accuracy of estimating VTEC at each station using VGOS data was between 1.0 and 5.8 TEC Units (TECU).

Keywords: Ionosphere, VLBI, VGOS, VTEC, GIM, CONT17

Plain Language Summary:

Ionosphere is the upper layer of the atmosphere, where free ions and electrons bend the extragalactic radio waves, which are received at ground stations. Such radio waves can be exploited for positioning or detection of Earth's crustal movements; thus, detecting the ionospheric effect on these signals is of paramount importance. This paper investigates the effects of this medium on the signals emitted from celestial bodies called "quasars" and received by

a system called Very Long Baseline Interferometry (VLBI) Global Observing System (VGOS) which is a new generation of. VLBI. Being inspired by Hobiger et al. (2006), we used a station-dependent model to estimate the temporal variation of the ionospheric Total Electron Content (TEC). Our initial results showed that there was an unreported error in the VGOS data, during CONT17 campaign of which we took account. We also enhanced the station-dependent model so that it could achieve a better estimation of TEC.

1- Introduction

The design of VGOS (VLBI Global Observing System) addresses many deficiencies of legacy VLBI system: it has small antennas that can slew between sources quickly, and it enjoys the broadband technology that increases sensitivity to allow short observations for better coverage of the ever-changing atmosphere (Petrachenko et al., 2009). The broadband characteristic of VGOS and how the broadband delay is obtained allows ionosphere contributions to be estimated more accurately. Instead of using the S and X bands of geodetic VLBI systems, broadband technology uses a range of frequencies (2-14 GHz) such that four bands with the least Radio Frequency Interference (RFI) can be chosen within this range. Coherently combining the data from these four bands and two polarizations allows the delay precision of single observations to be better than 16 ps (1 ps = 10^{-12} s) (Niell et al., 2018). Using this system, the baseline length estimates can be as precise as 0.3 mm. For a more detailed description of the VGOS system and its contribution to geodetic VLBI, see Niell et al. (2018).

The focal point of this paper lies in a new way to calculate ionospheric parameters. In legacy S/X VLBI systems utilizing X- and S-band, the differential delay caused by the ionosphere is removed by forming a linear combination of the S and X band group delays. This procedure is done after the correlation stage. Instead, in the VGOS data pipeline, estimates of dTEC (differential Total Electron Content) for each baseline are made during the correlation post-processing (Cappallo, 2015). For legacy S/X systems Hobiger et al. (2006) came up with a station-dependent model for estimating the frequency-dependent delay caused by the ionosphere and thus extracting the time series of Vertical Total Electron Content (VTEC) for each of the stations. The technique described in this paper is inspired by the Hobiger et al. (2006) model because it's not dependent on any external data other than VLBI, but still estimates the variation of the VTEC parameter during the observing session. Since VGOS is a new technique and is in a number of ways more complex than the legacy S/X systems, subtleties are arising from phase calibration and dTEC estimation that had to be taken into account in our analysis. Moreover, the model presented by Hobiger et al. (2006) considered only one unknown parameter for the latitude gradient of the ionosphere. In this study, however, this assumption is enhanced by introducing a time series for ionosphere latitude gradient. Another difference is that we used dTEC as the input data to estimate VTEC above each station point, whereas Hobiger et al. (2006) used ionospheric delay for this purpose.

2- Method

2-1- Extraction and Modeling of the Ionospheric Parameters

Interferometric systems such as S/X VLBI or VGOS are used to observe the difference in the interferometric phase of a noise signal from an extragalactic radio source, as received at two different antennas. Although the principal geodetic observable is group delay, the precision and wide frequency coverage of the VGOS observations necessitate accounting for the ionospheric effect at the post-correlation analysis stage. The phase model used in this stage is (Cappallo, 2016):

$$\phi(f) = \tau_g * (f - f_0) + \phi_0 - \frac{1.3445 * \mathrm{d}TEC}{f} \quad (1)$$

where ϕ is the interferometric phase (rotation), τ_g is the group delay (ns), f is frequency (GHz), f_0 is the *fourfit* reference frequency (GHz), ϕ_0 is the instrumental phase (rotation) at f_0, and *dTEC* is the differential TEC (TECU ≡ 10^{16}/m^2. Among other parameters, for each observation a value for τ_g and *dTEC* is estimated; this study uses those estimates of dTEC as our raw observable. Since our raw data come from the output of the *fourfit* program, it is useful to study in depth how dTEC is retrieved.

The model used by the correlator has imperfectly known physical parameters, such as source and station coordinates, station clock, and a non-hydrostatic part of the troposphere delay zenith wet delay). The estimates of each parameter contain errors and thus increase the total error. As a result, there are non-zero *residual delays* and *delay-rates. Fringe-fitting* is a post-correlation process that is responsible for correcting the errors of the estimates (e.g. Cotton, 1995). Based on equation (1), the parameter values (dTEC and the group delay) are adjusted within *fourfit*, in a manner such that all of the channel phases are as similar as possible, resulting in the greatest coherent sum of the individual channel phasors. (Cappallo, 2017).

Assuming small errors in the *a priori* parameters, the change in phase (to first order) can be written:

$$\Delta\phi(t,f) = \phi_0 + \left(\frac{\partial\phi}{\partial f}\Delta f\right) + \left(\frac{\partial\phi}{\partial t}\Delta t\right) \quad (2)$$

where ϕ_0 is the phase at reference time and frequency, $\frac{\partial\phi}{\partial f}$ is the residual group delay and $\frac{\partial\phi}{\partial t}$ is the residual fringe rate. equation (2) is also called the resolution function, which is to be maximized by finding the optimal group delay and fringe rate (Rogers,1970). The optimal delay and fringe rate are found through a search of coherently-summed amplitudes, over a 3-dimensional grid with axes denoting single-band delay (the group delay within each frequency channel), multi-band delay (the group delay after tying together the phases across all frequency channels), and group delay-fringe rate (simply delay-rate) (see, e.g., Cotton, 1995). VGOS fringe fitting for an experiment requires multiple setup runs of the program *fourfit* under different configurations, to correct channel phase offsets and find delay offsets for the bands. Within each scan, polarizations are coherently combined, and a fit is performed, yielding a set of calibrated broadband VGOS observables. The independent parameters that are estimated are interferometer phase, group delay, group delay-fringe rate, and dTEC (see equation (1)) and they are adjusted such that the coherently summed (over all channels) complex fringe amplitude is at a maximum.

Ideally, the phase calibration tones would allow the automatic adjustment of channel phases to achieve maximum coherence. In practice, though, particularly during the early period of VGOS due to the presence of hardware problems, it is necessary to make some "manual" adjustments to the channel phases. During the so-called manual phase calibration, the correlator engineer picks several strong scans and determines channel-by-channel phase offsets to maximize the fringes. Unfortunately, this has been shown to introduce small frequency-independent phase signatures, which mimic the effect of ionospheric dispersion. In essence, each station has a small, unknown, yet constant TEC value added to every observation. This makes it necessary to estimate and remove the effect of this *dispersion offset*.

As shown in equation (1), the phase contribution (in radians) due to the ionosphere is:

$$\Delta\phi = -1.3445 * \frac{\mathrm{d}TEC}{f} \quad (3)$$

where *dTEC* is the difference of TEC (in TEC units) above the two stations and the phase offset is applied to each individual frequency channel (Cappallo, 2017). The method used in *fourfit* to determine dTEC is to successively estimate the other independent parameters (phase, delay, and delay rate) at a grid of fixed values of dTEC that span a specified range. For each trial value of dTEC, a complete fringe fit is performed and from these fits, the interpolated maximum is found. The chosen value of dTEC (at the optimal value of delay and rate) maximizes the coherent sum of complex cross-spectral power. Note that for VGOS the cross-power spectra from the correlator need to be combined prior to the fringe-fit. Due to the use of linearly-polarized feeds, there are four complex correlation products (XX, YY, XY, YX), which are co-added into a Stokes Intensity equivalent, taking into account the parallactic angles of the antenna feeds (Cappallo, 2016).
The ionosphere is a dispersive medium in which signals are both refracted and delayed in a frequency-dependent manner (Böhm and Schuh, 2013). In the current study, we ignore ionospheric refraction, as well as the higher order terms of ionospheric delay (Hawarey et al., 2005), as they are currently below our sensitivity level.

The differential ionosphere can be treated as the difference of the TEC along the two slanted ray paths, $STEC_i$

$$dTEC = STEC_2 - STEC_1 \quad (4)$$

We will treat the ionosphere as a thin shell (Single Layer Model), as outlined in Fig. 1. This model assumes that all free electrons are concentrated in a shell of infinitesimal thickness, having an elevation angle dependence given by a mapping function. Furthermore, we assume a frozen-flow model, in which the distribution of the ionospheric density rotates with the sun, changing only slowly. By doing so, we can treat the offset in longitude of the pierce point relative to the station as an equivalent observation with the time tag adjusted to give the same solar time. The change in TEC due to an offset in the latitude of the pierce point will be an estimated parameter and will be described below.

2-2- Formulation of the Theoretical Model

The geometry of our observations can be seen in Figure 1, where the nomenclature of STEC* and VTEC* is utilized to explicitly denote the quantities at the ionospheric pierce point.

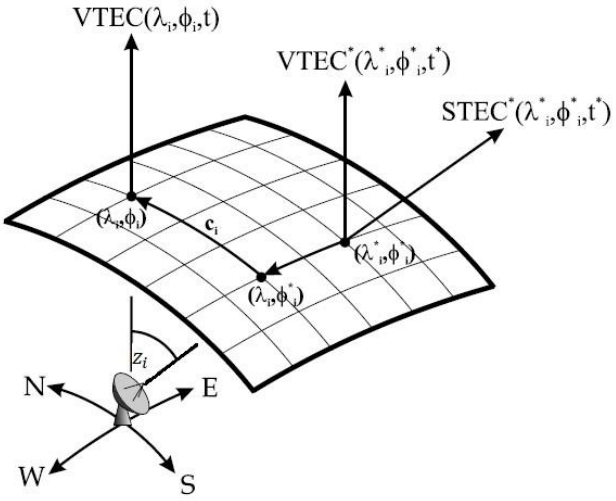

Fig. 1 The ionospheric pierce point (IPP) and offset coordinates (taken from Hobiger et al., 2006). Quantities with * superscript refer to the IPP. The longitude offset, $\lambda_i^*-\lambda_i$, is compensated for by changing the observation timetag. The gradient of TEC in latitude, c_i, is solved for, and multiplied by the latitude offset,$\phi_i^*-\phi_i$.

Our model consists of three components: for each station, there is a time series representing VTEC above that station, another time series for the latitude gradient of VTEC, and a dispersion offset. Both, the VTEC and latitude gradient time series are implemented as piecewise-linear polynomials; the model estimates the values of the endpoints of each connected segment. Specifically, if the endpoints are a set of (n+1) values having coordinates (t_k, a_k), with k running from 0 through n, when t lies in the interval [t_k, t_{k+1}] the piecewise-linear function *p(t)* is given by:

$$p(t) = \frac{(t_{k+1}-t)*a_k+(t-t_k)*a_{k+1}}{t_{k+1}-t_k} \quad (5)$$

Since the ray path travels obliquely through the ionospheric shell, its path length is increased. We can define a multiplicative factor F(z), which depends on the zenith angle.

$$F(z) = \frac{STEC}{VTEC} \quad (6)$$

A common choice for this function would be the Chapman mapping function which is based on the Single Layer Model (SLM) of the ionosphere (Schaer, 1999):

$$F(z) = \frac{1}{\sqrt{1-\left(\frac{R_E}{R_E+H}\sin z\right)^2}} \quad (7)$$

where R_E is the Earth radius, z is zenith angle and H is the height of the ionosphere layer. In order to be comparable with Center of Orbit Determination of Europe (CODE)'s data which we use as the reference in this work (see section 4), we adopted the Modified SLM (MSLM) (Schaer, 1999):

$$F_M(\mathrm{z}) = \frac{1}{\sqrt{1-\left(\frac{\mathrm{R_E}}{\mathrm{R_E+H}}\sin(\alpha \mathrm{z})\right)^2}} \quad (8)$$

where $\alpha = 0.9782$ is the scaling factor, and H= 506.7. The observation equation then becomes:

$$dTEC = \left(F(z_2) * VTEC_2(t_2^*) - F(z_1) * VTEC_1(t_1^*)\right) + c_2(t_2^*) * \Delta\phi_2 - c_1(t_1^*) * \Delta\phi_1 + \delta_2 - \delta_1 \quad (9)$$

where $VTEC_i$ is the piecewise-linear function for VTEC, $c_i(t)$ is the piecewise-linear latitude gradient function (in TECU/deg), and δ_i is the dispersion offset. These variables comprise the complete set of unknowns. Note that the evaluation times for the VTEC and c functions are offset to compensate for the time it takes the frozen pattern to rotate from the pierce point to the station's longitude, i.e. $t_i^* = t + \frac{\Delta\lambda_i}{15}$, i=1,2. No variation in longitude is explicitly solved for – changes in longitude only enter implicitly through the time dependency of c(t) and VTEC(t) (Dettmering et al., 2011). The intervals for the piecewise-linear function are chosen to be short enough to track the ionosphere variations, yet not be so long that the quality of the fit deteriorates as it becomes under-determined. In this study, due to the high observation temporal resolution of one minute or less, each group of 15 sequential observations represent one interval (Hobiger et al., 2006).

To perform a Least-Squares fit, we need to form a residual vector and minimize the squared sum of these residuals weighted by a weight matrix. If we define the $\Delta\boldsymbol{x}$ as unknowns, $\boldsymbol{A}$ as design matrix, $\Delta\boldsymbol{Y}$ as *observed minus calculated* vector, $\boldsymbol{v} = \boldsymbol{A}\Delta\boldsymbol{x} - \Delta\boldsymbol{Y}$ as residuals and $\boldsymbol{P}$ as the weight matrix (which is inversely proportional to the square of observations uncertainty), by minimizing $\boldsymbol{v}^T\boldsymbol{P}\boldsymbol{v}$ the problem will be solved as seen in equation (10). The derivatives with respect to $\Delta\boldsymbol{x}$ must be set to zero (Koch, 1997).

$$\min \boldsymbol{v}^T\boldsymbol{P}\boldsymbol{v} = \min(\Delta\boldsymbol{x}^T A^T\boldsymbol{P}\boldsymbol{A}\Delta\boldsymbol{x} - 2\boldsymbol{A}^T\boldsymbol{P}\Delta\boldsymbol{Y}\Delta\boldsymbol{x} + \Delta\boldsymbol{Y}^T\boldsymbol{P}\Delta\boldsymbol{Y}) \quad (10)$$

The dispersion offsets make the design matrix singular, as VLBI only makes differential delay measurements; hence to resolve them the additional constraint is placed that the sum of all station dispersion offsets is equal to zero.

$$\sum_{i=1}^{N} \delta_i = 0 \quad (11)$$

where N is the number of stations.

Using the formulation detailed above we extended the work of Hobiger et al. (2006). The fundamental input datum in Hobiger et al. (2006) is the ionospheric delay ($\tau_X - \tau$), but in the VGOS analysis, we work directly with TEC's, starting the processing with dTEC that is found in the "Observables" folder of the data in the vgosDB file format (for more information about vgosDB format, see Gipson (2015)), alongside its formal error of about 0.04 TECU reported by the *fourfit* program. The analysis described above is performed using MATLAB.

3- Data and Processing

Vienna VLBI Software (VieVS) was developed at the Vienna University of Technology (TU Wien) using MATLAB software and has been used extensively for analyzing VLBI data. After processing each session, a mat-structure file is stored in which all scans are organized sequentially, from which VTEC above each station can be extracted (Böhm et al., 2018).

For this study, we initially used VieVS to process the VGOS sessions, acquired in the CONT17 campaign (see Behrend et al. (2020)) and then, using the mat-structure file obtained by VieVS, applied the algorithm mentioned in section 2-2 for deriving VTEC and latitude gradient values from this dataset. This campaign, carried out by IVS, took place over a time period of about two weeks that only about a third of which, 5 days from the interval 3-8 December 2017, were observed with a VGOS broadband network. Principally we used data from the 3 December session to construct TEC and its latitude gradient above each station, although other sessions were processed for comparison. The stations that participated in this campaign were the Goddard Geophysical and Astronomical Observatory (GGAO12M), Westford (WESTFORD), and Kokee (KOKEE12M) in the United States, Ishioka (ISHIOKA) in Japan, Yebes (RAEGYEB) in Spain, and Wettzell (WETTZ13S) in Germany. Their geographical distribution can be seen in Fig. 2. In this campaign, antennas and VGOS backends were used to observe in 4 bands, each of which consisted of 8 dual-polarization (linear X & Y) 32 MHz wide channels. In this campaign, the Haystack Observatory Post-processing Software (HOPS) was used to determine dTEC values (Whitney et al., 2013).

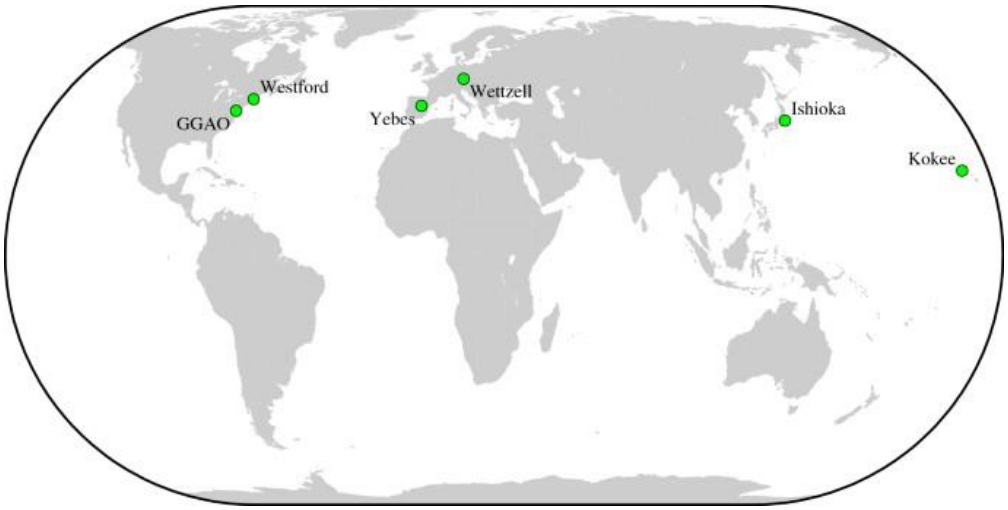

Fig. 2 The green points depict the stations that participated in the CONT17 campaign (Behrend et al., 2020)

4- Results and Discussion

Using the equations and techniques outlined in section 2-2, the VTEC and its latitudinal gradient time series above each of these six stations were estimated from dTEC data. To validate these results, the Global Ionosphere Maps (GIM) from the Center of Orbit Determination of Europe (CODE) which are issued in standard IONEX (IONosphere Map Exchange) format were used. The GIM is a global ionosphere map, providing VTEC from observations of GPS and GLONASS satellites. These files provide global values of VTEC every 2hour with the spatial resolution of 2.5 degrees in latitude and 5 degrees in longitude (Schaer et al., 1998). Interpolating to the coordinates of the CONT17 VGOS stations, the VTEC time series above each station was calculated from the map data. Alongside the VTEC grid, the Root Mean Squares (RMS) of these estimations are reported, which yield the formal error of the value of VTEC at each grid point. The accuracy cited for the GIM data varies with position and time, but it is generally within ±2 to ±8 TECU, for land and ocean stations respectively (Oceanic sites have degraded accuracy due to the sparsity of sites. For more information, see http://www.igs.org/products/data).

Our first efforts at comparing VGOS results and GIM data showed that the VTEC patterns tracked each other poorly. To find the source for this disagreement, we employed a closure constraint to examine the dTEC fidelity. All the possible triangles of baselines were considered to check that the dTEC values closed around a loop. The results clearly indicated that there were some problems with the input data. After thorough investigations, we concluded the following:

1- The VGOS antennas receive and process signals in two orthogonal linear polarizations. These polarized signals follow independent signal paths once they are separated at the feed: they are amplified, filtered, and digitized independently and the digital signals are carried on separate fibers. As a result, there is typically a small delay between the two senses of polarization, which needs to be removed properly in post-processing. Small errors in determining and applying this delay, coupled with small errors due to source structure effects and errors in phase calibration may cause a phase curvature across frequency that is mistakenly lumped into a dTEC contribution.

2- Some of the radio sources (e.g. 0552+398) have large structure effects when observed on the VGOS baselines. They are spatially extended; some of them have two-point structures and the others have multiple-point structures (Charlot, 1990). At the milli-arcsecond level, most of these sources exhibit time-variable extended structures and therefore are not ideal targets for geodetic applications unless this structure can be accounted for. As it can be seen in Charlot (1990) the phase curvature will be affected by this error source and according to equation (3), dTEC values will be changed as well.

3- The ionosphere is not always well-determined in the fringe fitting process. Due to the effects noted above, there can be multiple local maxima in the fringe amplitude near the "true" value of the dTEC. Sometimes these nearby maxima are larger than the correct peak and are thus chosen by *fourfit*.

4- Some of the signals (135 observations among 1180 observations) had poor SNR. The data pipeline did not filter upon a threshold for SNR value, whereas all of the signals with the SNR less than 7 must be discarded (The high threshold of an SNR of 7 takes into consideration the 'trials factor': since millions of individual points are searched in delay & rate space, detection needs to be 7 sigma or more to be significant. This threshold only works for VGOS observations, while in the case of legacy VLBI, thresholds for X- and S-bands are typically higher). A least-squares estimator has been used to derive the VTEC values from the dTEC data. Due to their potential strong effect on the solution, it was important to eliminate "blunder" points prior to fitting.

5- The most significant error was found (by one of the authors, Roger Cappallo, who is also a principal author of *fourfit*) in the sign of the dTEC value reported by *fourfit*. Essentially, the value reported had an inverted sign due to an incorrect implicit ordering of the stations comprising the baseline. Since dTEC is in some sense a 'nuisance parameter' to *fourfit*, a program that is primarily concerned with providing the best estimate of group delay, all dTEC values reported by *fourfit* have inadvertently had the opposite baseline difference sense from the other parameters. Within *fourfit* the code used the differenced value of dTEC with a compensating sign change so that there was no adverse effect on the geodetic observables; only the value of dTEC in the output data files had the unexpected sign.

Based upon the problems noted above, the analysis code was modified. After flipping the signs of dTEC to solve the 5 problem, filtering out points having dTEC misclosures with a magnitude of more than 1 TECU to overcome 1 to 3 error sources, and removing observations with low SNR for the 4 mentioned problem, the data were reprocessed. Table 1 shows the number of useful observations made in each station during CONT17 Campaign. The number of observations during 4 and 6 December is clearly less than other sessions, due to the lack of observations from the RAEGYEB and WESTFORD stations. According to the information in log-files of these sessions, WESTFORD had difficulty slewing to sources on 6 December, which lead to fewer observations. Also during this time, RAEGYEB encountered pointing and instrumental stability problems, which reduced the antenna's sensitivity to observe sources.

Station name	3 December	4 December	5 December	6 December	7 December
GGAO12M	2694	1910	2134	1927	2256
ISHIOKA	1113	857	924	822	990
KOKEE12M	898	743	828	746	797
RAEGYEB	1850	449	877	829	940
WESTFORD	2527	1818	2013	1472	2114
WETTZ13S	1414	785	1058	1094	1177

Table 1 Number of observations after removing erratic data points

The resulting plots for 3 December 2017 are shown in Fig. 3. Moreover, the residuals and the standard deviations of our estimated VTEC for the same day, which range from 0.2 TECU to 7.8 TECU are provided in Fig. 4. The VTEC estimated from the first hour of observations in KOKEE (0-1 h) has a discontinuity, most likely arising from a blunder point in the dTEC data. In order to get a more consistent fit, the observations involving KOKEE in this period of time were deleted.

Table 2 shows the level of agreement between the VTEC estimation by VGOS observations and the IONEX format files for all of the sessions during CONT17. Moreover, the overall agreement between GIM and VGOS-derived

VTEC for each day and each station is provided. To facilitate comparison, the time resolution of the two data sets of Fig. 3 have been matched.

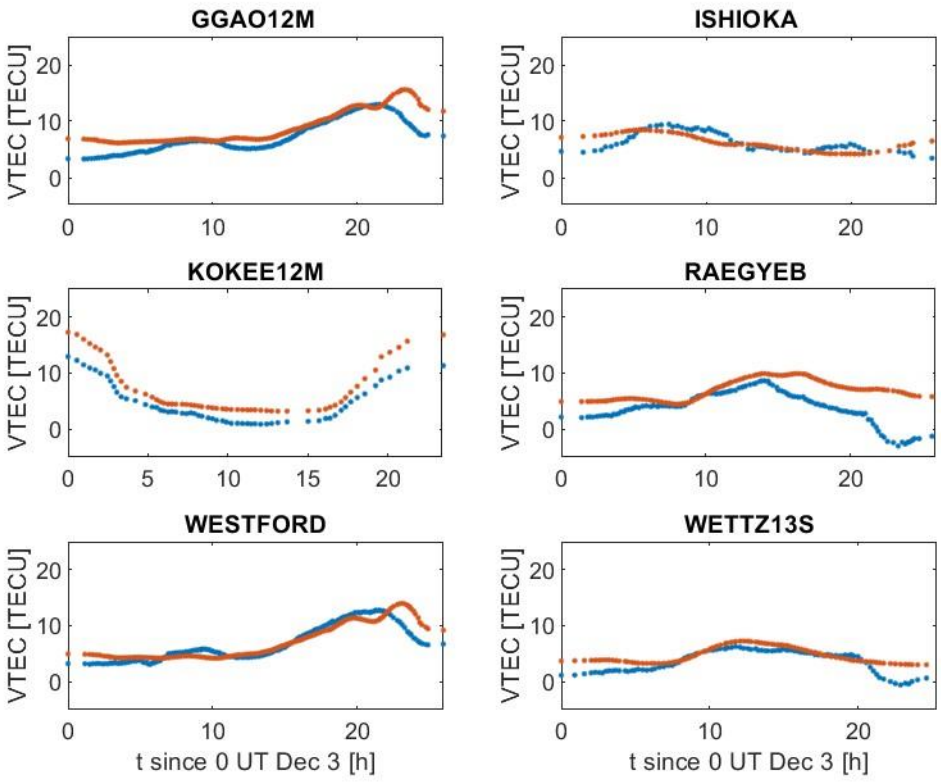

Fig. 3 Comparison of VTEC time series between VGOS (in blue) and GIM (in red) for 3 December session

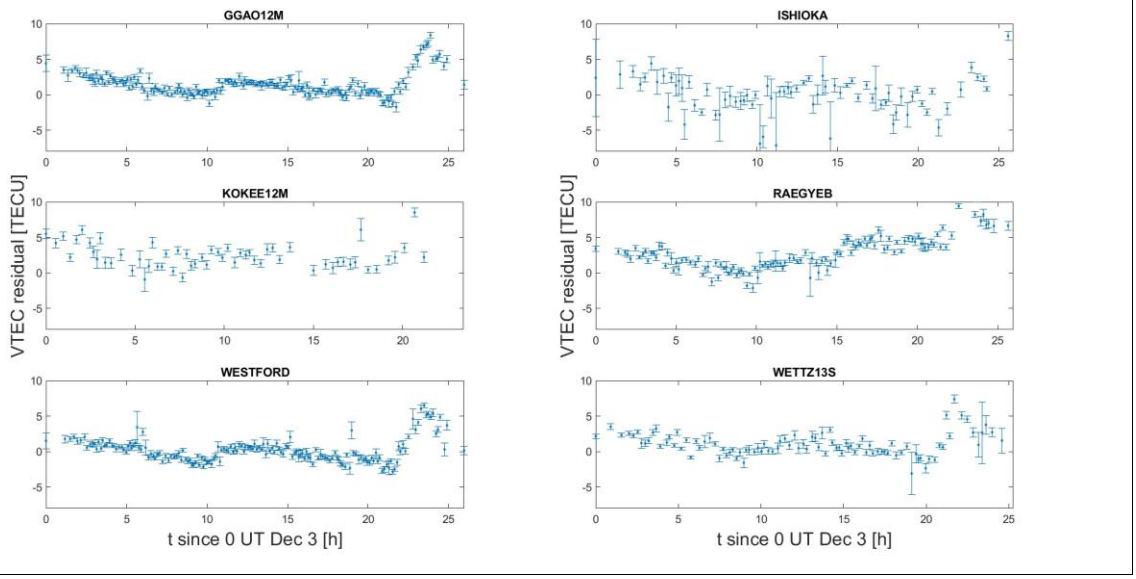

Fig. 4 Residuals (in the sense VGOS-GIM) with 1σ error bars from the VTEC estimation for each station for 3 December session

Station name	RMS (VTEC-IONEX) for 3 December (TECU)	RMS (VTEC-IONEX) for 4 December (TECU)	RMS (VTEC-IONEX) for 5 December (TECU)	RMS (VTEC-IONEX) for 6 December (TECU)	RMS (VTEC-IONEX) for 7 December (TECU)	Overall RMS (VTEC-IONEX) for each station (TECU)
GGAO12M	2.16	1.90	1.80	1.32	1.46	1.78
ISHIOKA	2.32	3.04	1.71	2.53	3.36	2.69
KOKEE12M	4.20	2.22	5.84	2.01	3.80	3.82
RAEGYEB	4.42	3.36	3.96	3.00	3.56	3.79
WESTFORD	1.57	1.77	1.67	1.10	1.06	1.47
WETTZ13S	2.00	2.10	1.64	1.30	2.19	1.89
Overall RMS (VTEC-IONEX) for each day (TECU)	2.80	2.23	2.77	1.81	2.39	

Table 2 RMS of VTEC differences (VGOS-GIM) per station for all of the sessions

As opposed to Hobiger et al. (2006), we did not use the non-negative constraint, because this would lead to a false negative bias in the final result. Thus, as can be seen in fig. 3, some points unexpectedly lie below zero. This is of course non-physcial, as the VTEC cannot take negative values. This disagreement can be due to several reasons. The phasecal at the RAEGYEB site was erratic, and in the post-processing a manual phase correction was made after the 12^{th} hour of the observations, the point at which the divergence from GIM data starts in Fig. 3. WETTZ13S experiences the same effect, but for a different reason, which is not totally understood, but may be related to unnoticed, and hence unfiltered, raw data points. Table 2 shows the discrepancy between VGOS and IONEX for all of the sessions and stations; KOKEE12M has the highest overall RMS (3.82 TECU) as it appears to have a large bias from the GIM data. In all of the sessions, the best fit can be achieved for WESTFORD, with an RMS of 1.47 TECU. Among the sessions of CONT17 campaign, 6 December has the best fit with GIM-based VTEC and the lowest RMS has occurred in 3 December session. Moreover, the range of the formal error of VTEC estimated from VGOS data during all sessions of CONT17 are provided in Table 3. Accordingly, ISHIOKA with the formal error of 12.99 TECU has the highest and GGAO12M with the formal error of 0.19 TECU has the lowest formal error of estimation.

Station name	Formal error of VGOS-derived VTEC for 3 December (TECU)	Formal error of VGOS-derived VTEC for 4 December (TECU)	Formal error of VGOS-derived VTEC for 5 December (TECU)	Formal error of VGOS-derived VTEC for 6 December (TECU)	Formal error of VGOS-derived VTEC for 7 December (TECU)
GGAO12M	0.20-1.25	0.30-1.11	0.22-0.67	0.26-0.81	0.19-2.41
ISHIOKA	0.29-7.48	0.34-12.99	0.33-1.84	0.31-5.29	0.26-7.41
KOKEE12M	0.46-1.67	0.40-1.74	0.34-1.45	0.37-1.04	0.32-1.52
RAEGYEB	0.27-2.65	0.72-1.95	0.57-1.87	0.57-1.91	0.43-1.32
WESTFORD	0.23-2.27	0.28-1.05	0.21-0.63	0.22-0.94	0.18-0.82
WETTZ13S	0.29-4.37	0.33-2.19	0.29-1.97	0.23-1.45	0.18-1.52

Table 3 The most and the least standard deviation of VTEC estimations using VGOS data during all the sessions of CONT17

Another set of parameters we estimate is the time series representing the latitude gradient. For comparison, the time series of VTEC latitude gradient obtained from GIM data (the red curve) and the estimated gradient time series (the blue curve) for 3 December 2017 are shown in Fig. 5. Consideration of Fig. 5 suggests that the variation of latitude gradients is sensible. Our analysis spans a 24 hours period and it seemed that considering a single parameter for the whole span, such as that used in Hobiger et al. (2006), is not a good solution, given the fluctuation of this parameter. Our estimated gradients are largely consistent with GIM data and their differences are mostly on the order of a few tens of percent of the effect. As seen in Fig. 6, where we show the residuals and the standard deviations of these parameters for 3 December 2017, KOKEE has the greatest disagreement compared to GIM results. This can be attributed to the fact that this station has the lowest latitude among stations involved in this campaign, and thus experiences a TEC that is both larger and more variable. We also note that ISHIOKA experiences the largest formal errors in the estimated latitude gradients. Since ISHIOKA is the station with the maximum longitude difference and thus all baselines are mostly oriented in east-west, it has poorer sampling in the N-S direction.

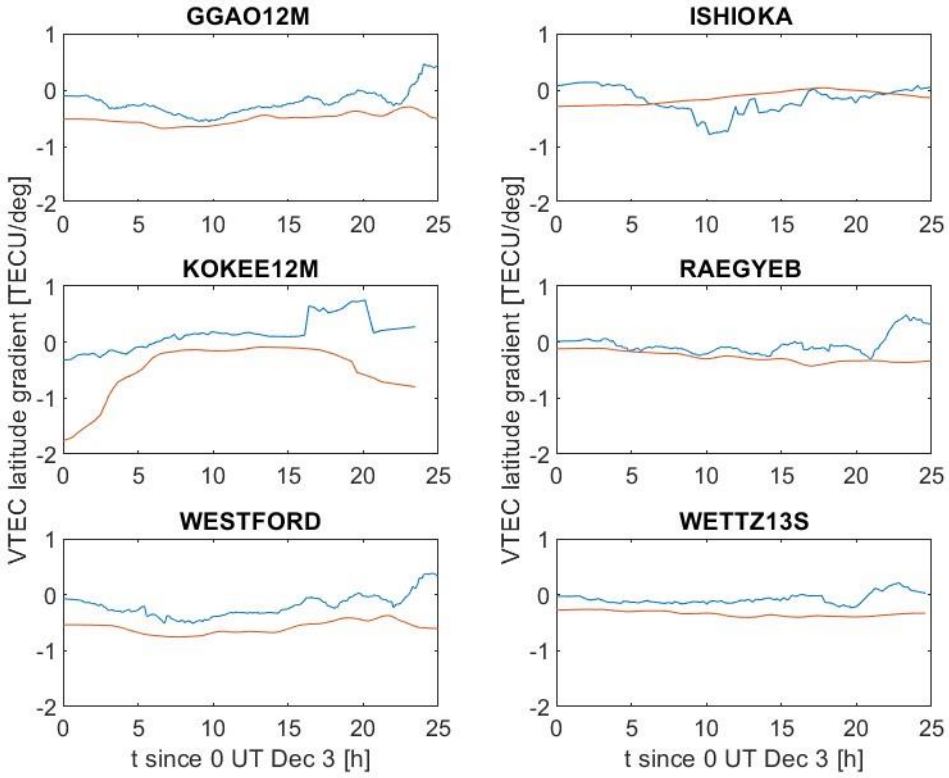

Fig. 5 Time series of latitude gradients based on GIM (blue line) versus the latitude gradients extracted from VGOS (red line) for 3 December session

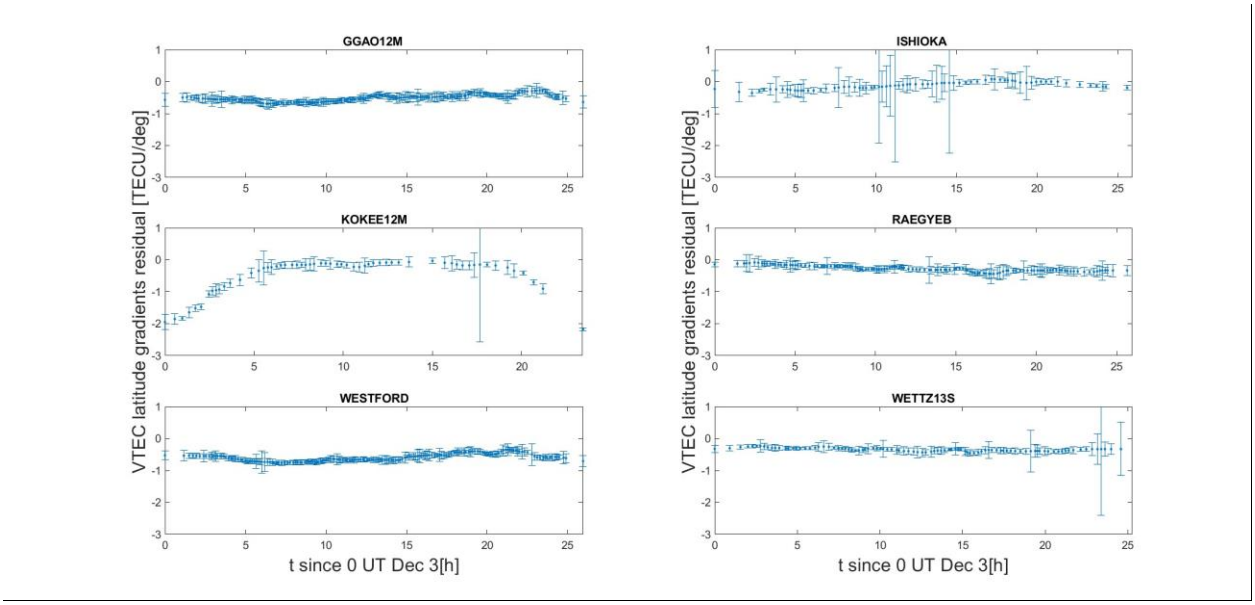

Fig. 6 Residuals (in the sense VGOS-GIM) with 1σ error bars from the latitude gradient estimations for each station for 3 December session

The internal error of GIM can affect the comparison, since this data set is the result of estimating spherical harmonic coefficients to create a grid map of VTEC over the world. Therefore, we compare the average formal error of each of the two methods for 3 December 2017 in Fig. 7. By interpolating the grid-wise RMS values provided in the IONEX file, the formal error of GIM data at each station point is obtained. As seen in this figure, for all of the stations the formal error of VTEC estimations appear to be lower than that of the GIM data. The RMS of the differences between the VTEC derived from VGOS and GIM data is also included in Fig. 7. Based on the statistical propagation of errors, the error of the sum of two independent and uncorrelated random variables is such that their variances add; i.e. if $Z = X - Y$, then $\sigma_Z^2 = \sigma_X^2 + \sigma_Y^2$. This is corresponding to the sum of the squares of blue and red bars being equal to the square of the orange bar. As can be seen in Fig. 7, the differences are larger than expected; the orange bar is larger than the root sum square of the blue and red bars. The implication is that either the error for one or both techniques are being underestimated, or that there is a non-noise-like systematic difference for which we're not accounting. Certainly the bias in the KOKEE data seems systematic.

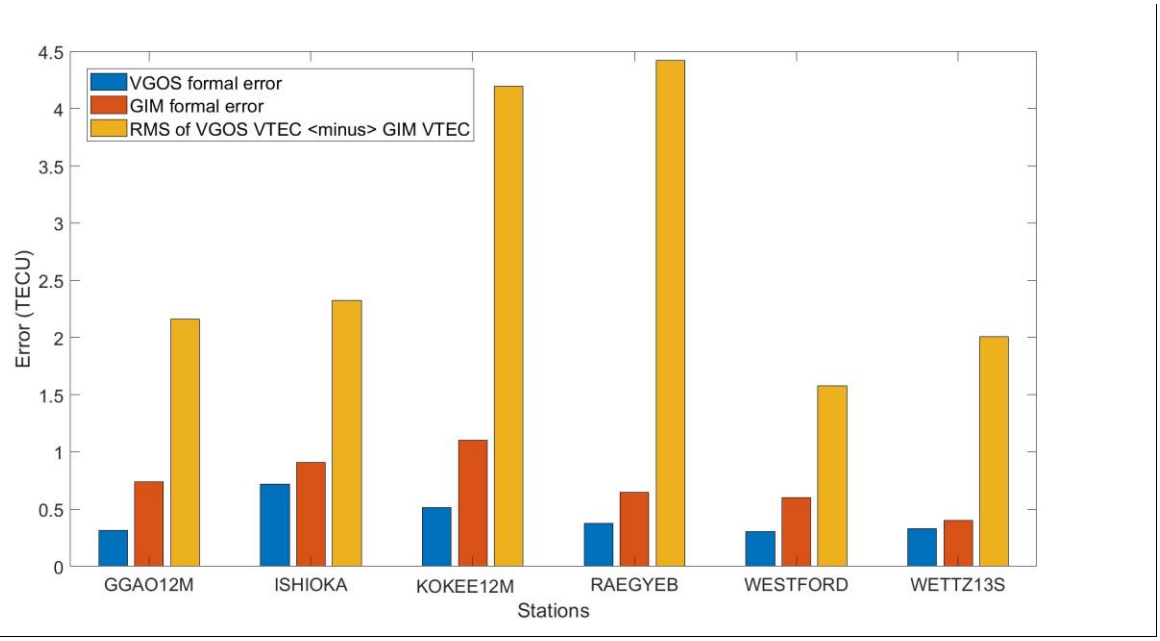

Fig. 7 The blue bars: the mean of formal error of VGOS-derived VTEC, the red bars: the mean of formal errors of GIM-based VTEC, and the orange bars: the RMS of VGOS <minus> GIM VTEC for 3 December

As it can be seen in Fig. 7, the VGOS formal error of VTEC above the KOKEE station, which is located in the ocean area, is (approximately 0.5 TECU) lower than GIM's formal error. This agrees with the fact that the accuracy of GIM-derived VTEC over the ocean area is much lower than for the inland area. Using this algorithm, four other sessions observed during CONT17 campaign were also processed; the results were consistent with the results of first day. For the sake of brevity, Figures 8 and 9 show the VTEC time series extracted from VGOS observations during 5 and 7 December sessions. Unlike the first day, the negative values for VTEC are not seen in the results of other days including 5 and 7 December, as the problem with phasecal in RAEGYEB was resolved for the consequent days.

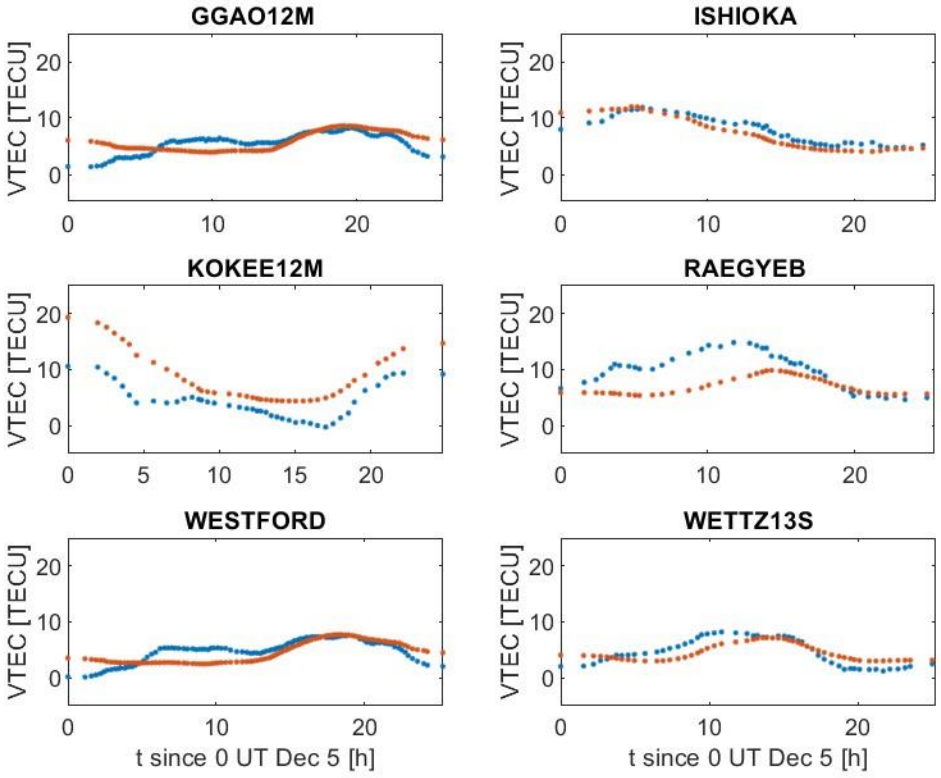

Fig. 8 Comparison of VTEC time series between VGOS (in blue) and GIM (in red) for 5 December session

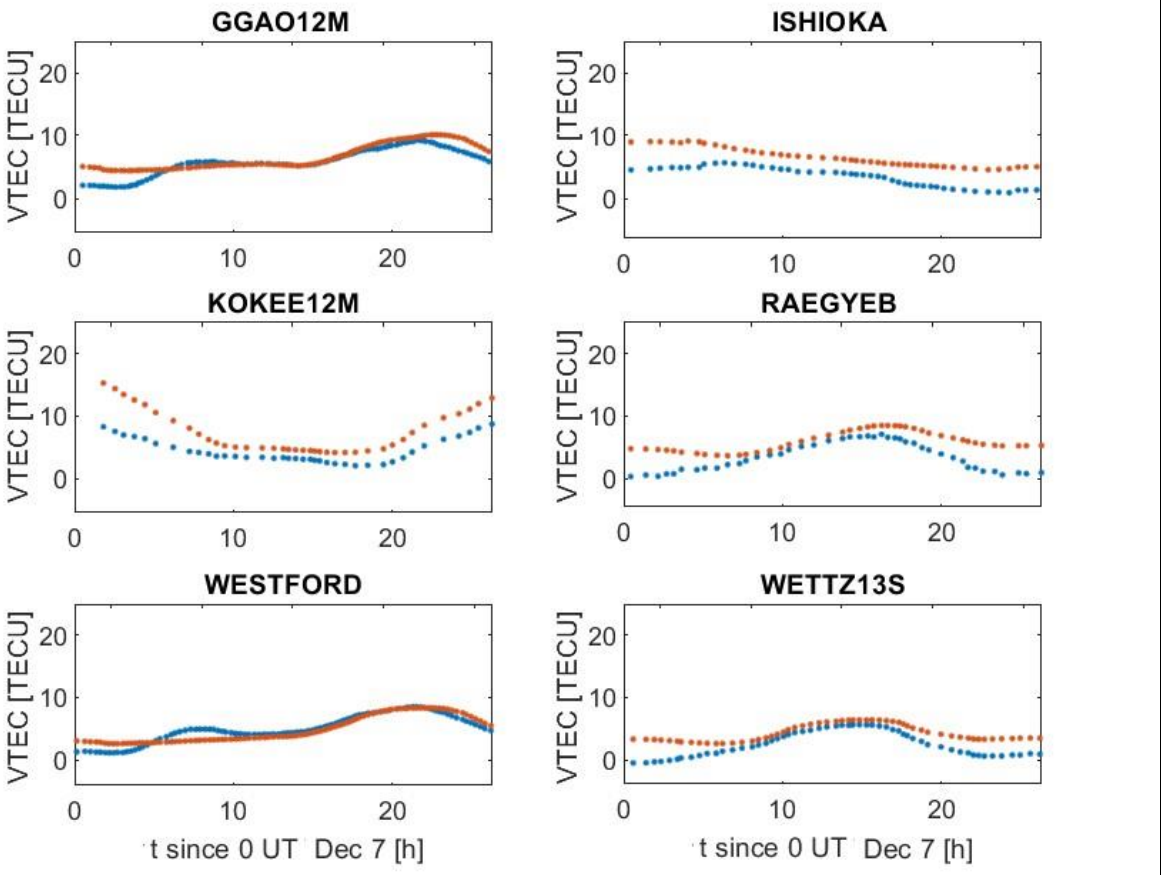

Fig. 9 Comparison of VTEC time series between VGOS (in blue) and GIM (in red) ionosphere for 7 December session

5- Summary and Conclusion

In this paper we tried station-dependent model on dTEC data to construct the time series of VTEC as well as the ionospheric latitude gradient above each station involved in CONT17 campaign. All dTEC observations in all 24-hour spans of VGOS data were processed and the VTEC values were extracted, and compared with CODE GIM. The dTEC data used in this investigation are parameters calculated by the *fourfit* program, with a typical formal error of 0.04 TECU. The method used in this research is inspired by the work of Hobiger et al. (2006), which was designed for group delay observations of S/X VLBI. Since this was the first time this method was applied to observations of the VGOS broadband system, many unexpected challenges arose, but ultimately the experience was successful. Even without comparison to the GIM model, the VTEC time series for 3 December session displayed in Fig. 3 are reasonable in general, because their peaks appear shortly after local noon (in which one sees the maximum solar activity and the largest TEC).

The standard deviation of VTEC estimated from VGOS data of all of CONT17 sessions is between 0.2 to 13 TECU and the level of agreement between VGOS-derived VTEC and GIM-based VTEC ranges from 1.0 to 5.8 TECU. Unsurprisingly, KOKEE station, which lies closest to the equator, experienced the greatest fluctuation in ionosphere activity and consequently has the worst accuracy in estimation of VTEC during the whole campaign (an RMS of 3.8 TECU). Among all days of CONT17 campaign, 3 December had the worst agreement with GIM-based VTEC (an RMS of 2.8) and 6 December had the best fit (an RMS of 1.8). During all VGOS sessions of CONT17, WESTFORD station had the best agreement with GIM values, with the overall RMS of 1.5 TECU.

Another set of estimates was the time series of latitude gradient of the ionosphere, which was compared to that of GIM-based values. The formal errors of the latitude gradients get larger at ISHIOKA, while KOKEE has the worst accuracy in determination of latitude gradient. As expected, KOKEE station also showed the worst accuracy in the VTEC GIM comparisons in all sessions, except for the first session in which RAEGYEB showed the highest RMS. One contributing factor might be the larger GIM error in oceanic zones. In addition, the VLBI observations sample the ionosphere at a given point in time and a specific direction, which the smoothed (in time and space) GIM model cannot predict.

From comparison of the first session results we saw that in all of the stations the formal errors of VTEC estimates using VGOS data were smaller than the formal error of GIM-derived VTEC. That does not necessarily mean that our estimations are better than GIM. Nevertheless, one benefit of the current study is to act as an independent check of the validity of the GIM model, which has very different signal sources, geometries, and processing methods.

Data Availability: VGOS data during CONT17 are available from https://ivscc.gsfc.nasa.gov/products-data/data.html and GIM data are accessible through https://cddis.nasa.gov/archive/gnss/products/ionex/.

6- Acknowledgments

This study is based upon work done by the first author as a part of the requirements of an MSc degree in K. N. Toosi University of Technology. The authors would like to thank three reviewers of Journal of Geodesy for their valuable comments. We also give credit to Dr. Sigrid Boehm, the head of the support team of VieVS software and express our appreciation to other colleagues at the MIT Haystack Observatory, namely, Anthea Coster, Mike Titus, and Geoffrey Crew, and from NVI Incorporated, John Gipson. We are grateful to all parties that contributed to the success of the CONT17 campaign, in particular to the IVS Coordinating Center at NASA Goddard Space Flight Center (GSFC) for taking the bulk of the organizational load, to the GSFC VLBI group for preparing the legacy S/X observing schedules and MIT Haystack Observatory for the VGOS observing schedules, to the IVS observing stations at Badary and Zelenchukskaya (both Institute for Applied Astronomy, IAA, St. Petersburg, Russia), Fortaleza (Rádio Observatório Espacial do Nordeste, ROEN; Center of Radio Astronomy and Astrophysics, Engineering School, Mackenzie Presbyterian University, Sao Paulo and Brazilian Instituto Nacional de Pesquisas Espaciais, INPE, Brazil), GGAO (MIT Haystack Observatory and NASA GSFC, USA), Hartebeesthoek (Hartebeesthoek Radio Astronomy Observatory, National Research Foundation, South Africa), the AuScope stations of Hobart, Katherine, and Yarragadee (Geoscience Australia, University of Tasmania), Ishioka (Geospatial Information Authority of Japan), Kashima (National Institute of Information and Communications Technology, Japan), Kokee Park (U.S. Naval Observatory and NASA GSFC, USA), Matera (Agencia Spatiale Italiana, Italy), Medicina (Istituto di Radioastronomia, Italy), Ny Ålesund (Kartverket, Norway), Onsala (Onsala Space Observatory, Chalmers University of Technology, Sweden), Seshan (Shanghai Astronomical Observatory, China), Warkworth (Auckland University of Technology, New Zealand), Westford (MIT Haystack Observatory), Wettzell (Bundesamt für Kartographie und Geodäsie and Technische Universität München, Germany), and Yebes (Instituto Geográfico Nacional, Spain) plus the Very Long Baseline Array (VLBA) stations of the Long Baseline Observatory (LBO) for carrying out the observations under the US Naval Observatory's time allocation, to the staff at the MPIfR/BKG correlator center, the VLBA correlator at Socorro, and the MIT Haystack Observatory correlator for performing the correlations and the fringe fitting of the data, and to the IVS Data Centers at BKG (Leipzig, Germany), Observatoire de Paris (France), and NASA CDDIS (Greenbelt, MD, USA) for the central data holds.

7- References

Behrend, D., Thomas, C., Gipson, J., Himwich, E., & Le Bail, K. (2020). On the organization of CONT17. *Journal of Geodesy*, 94(10), 1-13. http://doi.org/10.1007/s00190-020-01436-x

Böhm, J., Böhm, S., Boisits, J., Girdiuk, A., Gruber, J., Hellerschmied, A., et al. (2018). Vienna VLBI and satellite software (VieVS) for geodesy and astrometry. *Publications of the Astronomical Society of the Pacific*, 130(986), 044503. http://doi.org/10.1088/1538-3873/aaa22b

Böhm, J., & Schuh, H. (Eds.). (2013). *Atmospheric effects in space geodesy* (Vol. 5). Berlin: Springer. https://doi.org/10.1007/978-3-642-36932-2

Cappallo, R. (2015). Covariance analysis of the simultaneous fit of group delay and dTEC in fourfit. *Documentation of HOPS*, 1-5.

Cappallo, R. (2016, December). Delay and Phase Calibration in VGOS Post-Processing. In *IVS 2016 General Meeting Proceedings* (pp. 61-64).

Cappallo, R. (2017). FOURFIT user's manual.

Charlot, P. (1990). Radio-source structure in astrometric and geodetic very long baseline interferometry. *The Astronomical Journal*, *99*, 1309-1326. https://doi.org/10.1086/115419

Cotton, W. D. (1995). Fringe fitting. In *Very Long Baseline Interferometry and the VLBA* (Vol. 82, p. 189).

Dettmering, D., Heinkelmann, R., & Schmidt, M., 2011. Systematic differences between VTEC obtained by different space-geodetic techniques during CONT08. *Journal of Geodesy*, *85*(7), 443. https://doi.org/10.1007/s00190-011-0473-z

Gipson, J. (2015, November). Practical Uses of VGOSDB Format. In *Proceedings of the 22nd European VLBI Group for Geodesy and Astrometry Working Meeting 18-21 May 2015 Ponta Delgada* (pp. 97-101).

Hawarey, M., Hobiger, T., & Schuh, H. (2005). Effects of the 2nd order ionospheric terms on VLBI measurements. *Geophysical research letters*, *32*(11). https://doi.org/10.1029/2005GL022729

Hobiger, T., Kondo, T., & Schuh, H. (2006). Very long baseline interferometry as a tool to probe the ionosphere. *Radio Science*, *41*(01), 1-10. https://doi.org/10.1029/2005RS003297

Koch, K. R. (2013). *Parameter estimation and hypothesis testing in linear models*. Springer Science & Business Media. https://doi.org/10.1007/978-3-662-03976-2

Niell, A., Barrett, J., Burns, A., Cappallo, R., Corey, B., Derome, et al. (2018). Demonstration of a broadband very long baseline interferometer system: a new instrument for high-precision space geodesy. *Radio Science*, *53*(10), 1269-1291. https://doi.org/10.1029/2018RS006617

Petrachenko, B., Niell, A., Behrend, D., Corey, B., Böhm, J., Chralot, et al. (2009). *Design Aspects of the VLBI2010 System, Progress Report of the IVS VLBI2010 Committee, NASA*. TM-2009-214180.

Rogers, A. E. E. (1970). Very long baseline interferometry with large effective bandwidth for phase-delay measurements. *Radio Science*, *5*(10), 1239–1247. https://doi.org/10.1029/RS005i010p01239

Schaer, S., 1999. Mapping and predicting the Earth's ionosphere using the Global Positioning System, Ph.D. dissertation, Univ. Bern, Bern, Switzerland.

Schaer, S., Gurtner, W., & Feltens, J. (1998, February). IONEX: The ionosphere map exchange format version 1. In *Proceedings of the IGS AC workshop, Darmstadt, Germany* (Vol. 9, No. 11).

Whitney, A. R., Beaudoin, C. J., Cappallo, R. J., Corey, B. E., Crew, G. B., Doeleman, S. S., et al. (2013). Demonstration of a 16 Gbps per station broadband-RF VLBI system. *Publications of the Astronomical Society of the Pacific*, *125*(924), 196. https://doi.org/10.1086/669718